Advanced ZnO:Ce@GO nanocomposites for enhanced visible–light photocatalytic degradation of Disperse Red 152

Vu Huong Ly[1], Chu Manh Nhuong[1*], Duong Thanh Hoa[1], Bui Van Ly[2]

[1]Thai Nguyen University of Education, 20 Luong Ngoc Quyen, Phan Dinh Phung, Thai Nguyen, Vietnam;
[2]Dong Cac Primary and Secondary School, Dong Hung, Hung Yen, Vietnam.
[*]Corresponding author: nhuongcm@tnue.edu.vn
Received 15 Jan. 2026; Revised 13 Mar. 2026; Accepted 20 May 2026; Published 25 Jun. 2026.
DOI: https://doi.org/10.54939/1859-1043.j.mst.112.2026.108-115

ABSTRACT

ZnO and ZnO:Ce@(0–8)%GO nanocomposites were synthesized hydrothermally and characterized by XRD, FT–IR, PL, EDS, and UV–Vis–DRS. The materials retained the wurtzite ZnO structure with crystallite sizes of 28–38 nm. Ce doping and GO incorporation reduced the band gap from 3.15 to 2.78 eV and significantly suppressed electron–hole recombination, as evidenced by PL quenching. Under visible-light irradiation, ZnO:Ce@8%GO achieved 98.60% degradation of DR152 after 210 min, compared with 79.69% for pristine ZnO, with a reaction rate 2.94 times higher. The composite also retained 83.71% of its activity after five cycles, demonstrating good stability and the synergistic enhancement of photocatalytic performance by Ce and GO.

Keywords: ZnO:Ce@GO; Nanocomposite; Synergistic effect; Photocatalysis; Disperse Red 152.

1. INTRODUCTION

Zinc oxide (ZnO) is a semiconductor oxide with high chemical stability, large exciton binding energy (~60 meV), strong UV–visible absorption, low cost, and environmental friendliness [1-8]. However, its relatively wide band gap (~3.37 eV) and rapid recombination of photogenerated electron–hole pairs limit its photocatalytic efficiency [9-15]. Graphene oxide (GO), owing to its high surface area, enhanced electrical conductivity, and abundant oxygen-containing functional groups, can effectively improve charge transfer, suppress carrier recombination, and provide anchoring sites for metal oxide nanoparticles, thereby enhancing photocatalytic performance under solar irradiation [1, 3, 5, 6].

To overcome the intrinsic limitations of ZnO, various approaches have been developed, including coupling with other metal oxides and doping with metal ions from the d-, s-, and f-block elements [1–15]. These modifications can promote charge separation, increase oxygen-vacancy concentrations, and extend light absorption. For example, Songkot Utara et al. synthesized Zn-doped CeO_2/rGO nanocomposites with high surface area, reduced band gap, and abundant oxygen vacancies [3]. Moro Haruna et al. reported that Ce–ZnO–rGO nanocomposites achieved ~92% degradation of bromothymol blue under visible light owing to band-gap narrowing (~2.81 eV) [5]. Similarly, Ce-doped ZnO/rGO prepared by Patil and Nandibewoor exhibited excellent electrochemical sensing performance [6], while GO–ZnO/Mn_2O_3 composites showed a narrow band gap (~1.6 eV) and 98.75% degradation of malachite green under simulated sunlight [9].

Overall, ZnO-based nanocomposites offer tunable band structures, improved charge separation, and enhanced surface activity, making them promising materials for photocatalysis and environmental remediation. In this context, the present study focuses on the hydrothermal synthesis of ZnO:Ce@GO nanocomposites, their physicochemical properties, and their photocatalytic performance toward the degradation of Disperse Red 152 in aqueous solution.

2. EXPERIMENTAL

2.1. Chemicals, materials, and instrumentation

ZnO and ZnO:Ce@(0–8)%GO nanocomposites were synthesized by a hydrothermal method using $Zn(NO_3)_2$, $Ce(SO_4)_2{\cdot}4H_2O$, NH_3, and graphene oxide (GO), followed by filtration, washing, and calcination at 400 °C for 2 h. Their structural and optical properties were characterized by XRD, FT–IR, PL, UV–Vis–DRS, and EDS, while dye absorbance was determined using a UV–1700 spectrophotometer.

Photocatalytic experiments were carried out under simulated visible light irradiation generated by a 300 W xenon lamp. A UV-cut filter ($\lambda > 400$ nm) was employed to eliminate ultraviolet radiation and ensure visible-light-driven photocatalysis. The light source was positioned 10 cm above the reaction vessel, and all experiments were conducted in a dark chamber to prevent interference from ambient light.

2.2. Photocatalytic degradation of Disperse Red 152

Photocatalytic degradation of Disperse Red 152 (DR152) was performed by dispersing 25.0 mg of catalyst in 50 mL of DR152 solution (30.0 $mg{\cdot}L^{-1}$) containing 0.1 mL of 30% H_2O_2 in a 100 mL glass beaker. The suspension was stirred in the dark for 90 min to establish adsorption–desorption equilibrium, followed by visible-light irradiation for up to 210 min. All experiments were conducted in a dark chamber to eliminate interference from ambient light.

After treatment, the suspensions were centrifuged at 4000 rpm for 3 min, and the supernatants were analyzed by UV–Vis spectroscopy. The maximum absorbance of DR152 was observed at 528 nm. The degradation efficiency (%H) was calculated using Eq. (1), where A_0 and A are the absorbance values at the initial time and irradiation time *t* (min), respectively.

$$\%H = \frac{A_0 - A}{A_0}.100 = (1 - \frac{A}{A_0}).100 \quad (1)$$

3. RESULTS AND DISCUSSION

3.1. X-ray diffraction analysis of ZnO and ZnO:Ce@GO materials

Observation of the X-ray diffraction patterns in Figure 1 reveals that both ZnO and ZnO:Ce@(0–8)%GO materials exhibit well–defined diffraction peaks at $2\theta \approx 31.71°$, 34.35°, 36.21°, 47.48°, 56.51°, 62.78°, 66.32°, 67.87°, and 69.04°, which can be indexed to the (100), (002), (101), (102), (110), (103), (200), (112), and (201) crystallographic planes of the hexagonal wurtzite ZnO structure, in good agreement with the standard JCPDS card No. 036-1451 [1-5].

As shown in Figure 1b, the GO sample exhibits a characteristic (001) diffraction peak at $2\theta \approx 12.29°$ ($d_{001} \approx 0.8$ nm), confirming the presence of graphene oxide. Additional peaks at 26.47° and 43.61° correspond to the (002) and (100) planes of reduced graphene oxide (rGO), indicating partial thermal reduction of GO during calcination at 400 °C [1, 3, 6]. The coexistence of GO and rGO is expected to enhance electrical conductivity and facilitate electron transport, thereby improving charge separation.

Upon Ce doping and GO incorporation, the ZnO diffraction peak near $2\theta \approx 36°$ shifts slightly toward higher angles, indicating lattice modification caused by Ce–GO interactions. Although the wurtzite ZnO structure remains unchanged, the crystallite size increases from 28.24 to 38.46 nm, accompanied by a slight reduction in lattice parameters and unit-cell volume, with deviations of +0.52–3.02% relative to standard ZnO (47.62 $Å^3$) [4–8]. As shown in Table 1, the unit-cell volume decreases from 49.056 to 47.866 $Å^3$, whereas the crystallite size increases from 28.24 to 38.46 nm. These trends are consistent because unit-cell volume reflects atomic-scale lattice distortion, while crystallite size represents the growth of diffraction domains. The observed lattice contraction is likely related to oxygen-vacancy formation, internal strain, strong ZnO–GO interactions, and grain growth during calcination at 400 °C.

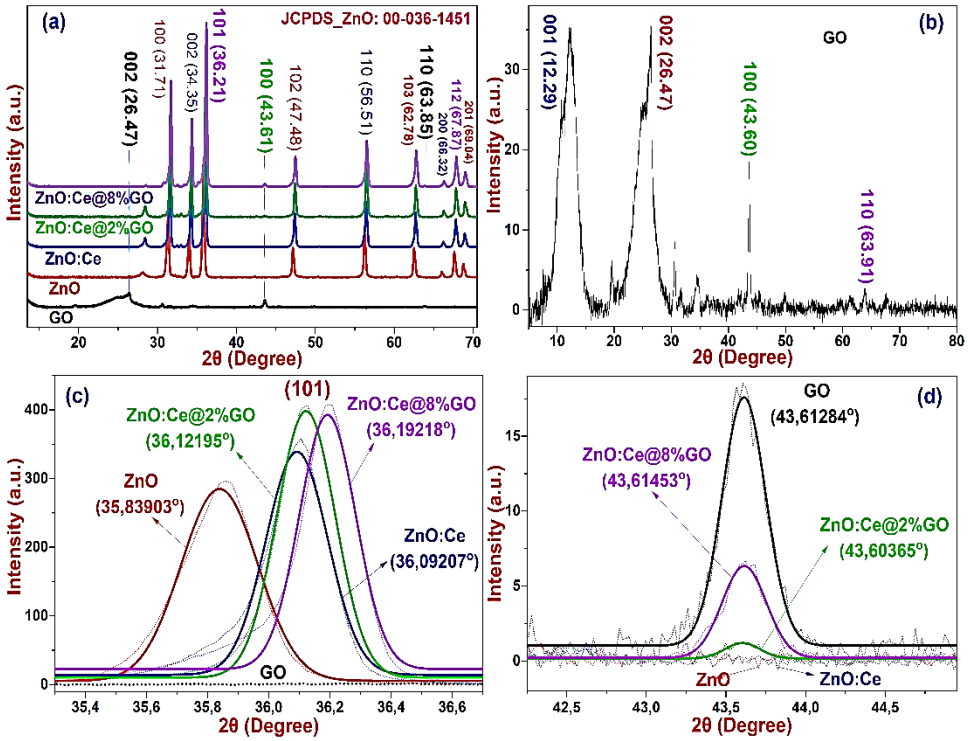

Figure 1. *XRD patterns and Gaussian peak fitting of GO, ZnO, and ZnO:Ce@(0–8)%GO.*

Table 1. *Average crystallite size (D) of GO, ZnO, and ZnO:Ce@x%GO (x = 0–8).*

	Crystal plane (101)			Crystal plane (100)			Lattice parameters		
	Diffraction angle 2θ (°)	FWHM (°)	D (nm)	Diffraction angle 2θ (°)	FWHM (°)	D (nm)	a (Å)	c (Å)	V (Å³)
GO	-	-	-	43.61284	0.32352	26.45	-	-	-
ZnO	35.83903	0.29564	28.24	-	-	-	3.2950	5.2172	49.056
ZnO:Ce	36.09207	0.23853	35.03	-	-	-	3.2661	5.2172	48.198
ZnO:Ce@2%GO	36.12195	0.22593	36.98	43.60365	0.25767	33.21	3.2627	5.2172	48.098
ZnO:Ce@8%GO	36.19218	0.21733	38.46	43.61453	0.32613	26.24	3.2548	5.2172	47.866

3.2. FT-IR spectra of ZnO and ZnO:Ce@(0–8)%GO

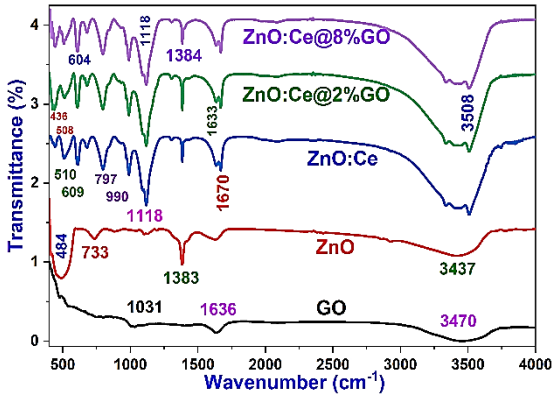

Figure 2. *FT–IR spectra of GO, ZnO, and ZnO:Ce@(0–8)%GO.*

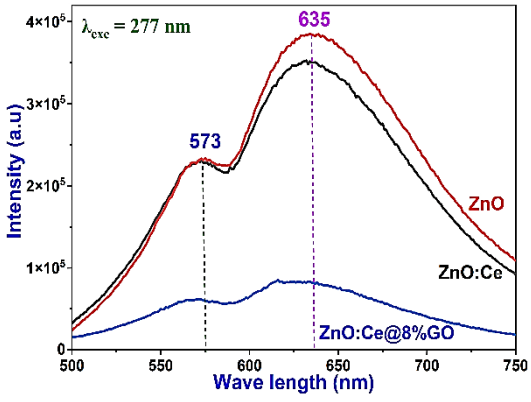

Figure 3. *PL spectra of ZnO nanoparticles and ZnO:Ce@(0–8)%GO nanocomposites.*

Figure 2 presents the FT–IR spectra of the materials in the range 4000 - 400 cm^{-1}. Characteristic Zn–O and O–Zn–O vibrations appear at ~ 436 - 510 cm^{-1} and ~ 609 - 797 cm^{-1}, respectively, while the broad band at ~3437 cm^{-1} is assigned to surface –OH groups from adsorbed water [10-14]. Compared with pristine ZnO, ZnO:Ce@(0–8)%GO shows slight peak shifts, indicating interactions among ZnO, Ce, and GO. The bands at ~1384 cm^{-1} (C–C), 1031 - 1118 cm^{-1} (C–O), and 1633 - 1670 cm^{-1} (C=O) further confirm the successful incorporation of GO and its oxygen-containing functional groups [1, 5, 15].

3.3. Photoluminescence spectra of the materials

Figure 3 presents the PL spectra of ZnO and ZnO:Ce@(0–8)%GO (λ_{exc} = 277 nm). Pristine ZnO shows strong emissions at ~573 and ~635 nm, attributed to intrinsic defects such as oxygen vacancies and surface states. Ce doping markedly reduces the PL intensity, indicating suppressed radiative recombination through charge trapping. The ZnO:Ce@8%GO sample exhibits the weakest emission due to efficient electron transfer from ZnO to GO. The decreasing PL intensity (ZnO > ZnO:Ce > ZnO:Ce@8%GO) confirms the synergistic role of Ce and GO in enhancing charge separation and promoting ROS generation for photocatalysis [9–12].

3.4. Optical properties and band gap energy of the materials

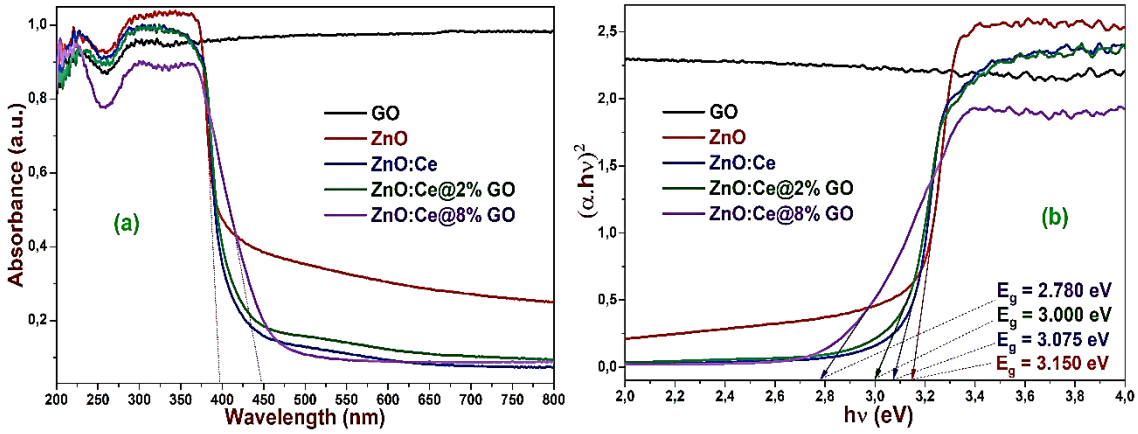

Figure 4. *(a) UV–Vis–Drs and (b) Tau'c plots of GO, ZnO and ZnO:Ce@(0–8)%GO.*

The UV–Vis–DRS spectra (Figure 4a) show a red shift of the absorption edge from ~394 to 446 nm after Ce and GO incorporation, extending light absorption into the visible region. Tauc analysis (Figure 4b) indicates that the band gap decreases from 3.15 to 2.78 eV, consistent with previous studies [3-8]. This behavior is attributed to Ce 4f states and improved charge transfer through GO, which together enhance visible-light photocatalytic activity.

3.5. Photocatalytic degradation of Disperse Red 152 (DR152) over ZnO and ZnO:Ce@(0–8)%GO photocatalysts

Figures 5(a–c) present the UV–Vis absorption spectra and concentration changes of DR152 during photocatalytic degradation over ZnO and ZnO:Ce@8%GO. The ZnO:Ce@8%GO samples exhibit significantly improved efficiency compared with pristine ZnO, increasing from 79.69% to 98.60%, demonstrating the synergistic effect of Ce^{4+} doping and GO hybridization.

Figures 6(a, b) show the variation of DR152 concentration with irradiation time and the corresponding pseudo–first–order kinetic plots for ZnO and ZnO:Ce@8%GO. The apparent rate constants are 6.120×10^{-3} and 1.777×10^{-2} min^{-1}, respectively, indicating that the activity of ZnO:Ce@8%GO is about 2.94 times higher than pristine ZnO under visible light. These results confirm the synergistic effect of Ce^{4+} and GO in enhancing charge separation and ROS generation ($^{\bullet}O_2^-$, $^{\bullet}OH$), thereby improving the photocatalytic degradation of DR152 [10-15].

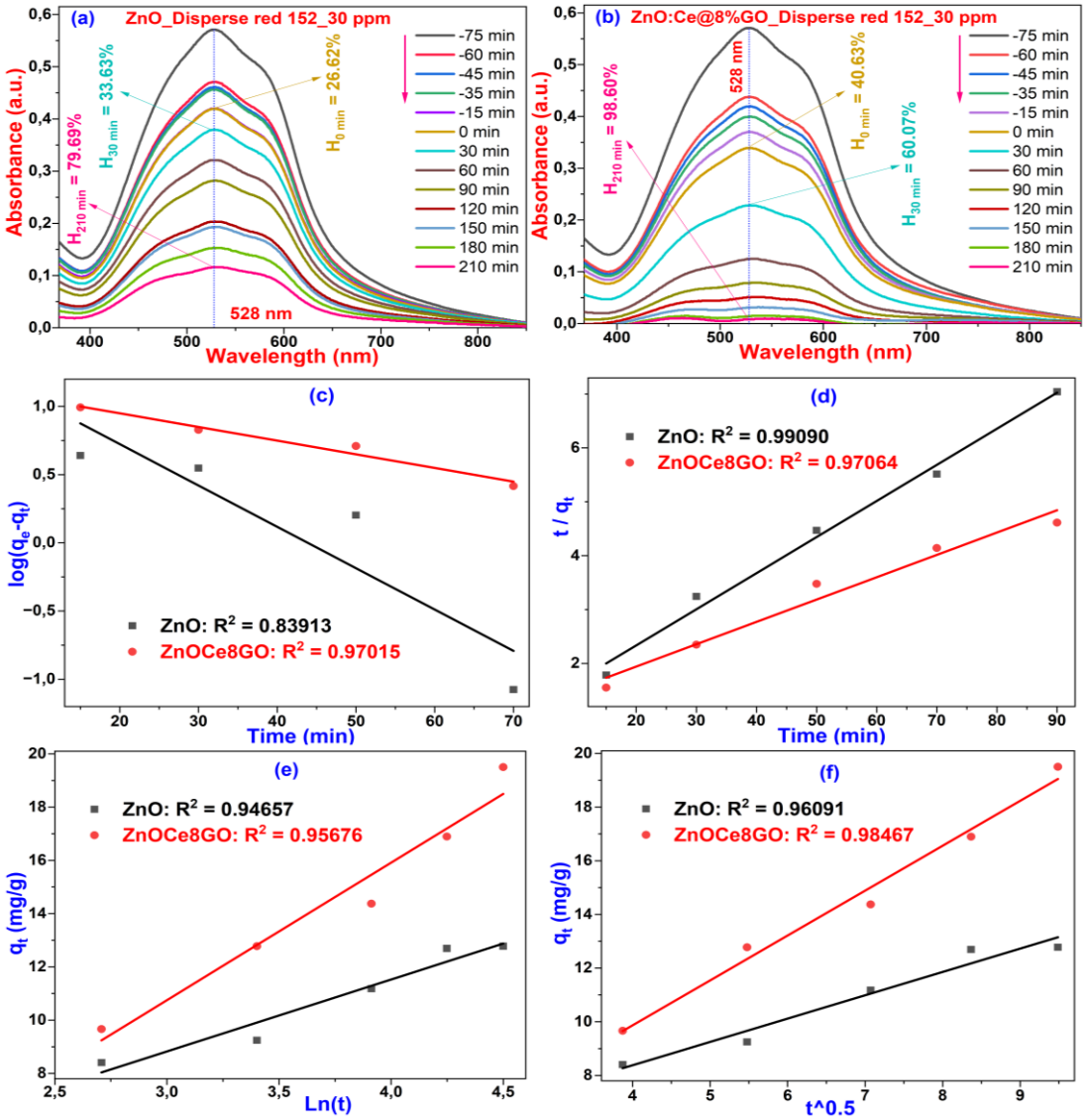

Figure 5. *Adsorption of DR152 on ZnO and ZnO:Ce@8%GO: (a,b) UV–Vis spectra and (c–f) kinetic model fittings.*

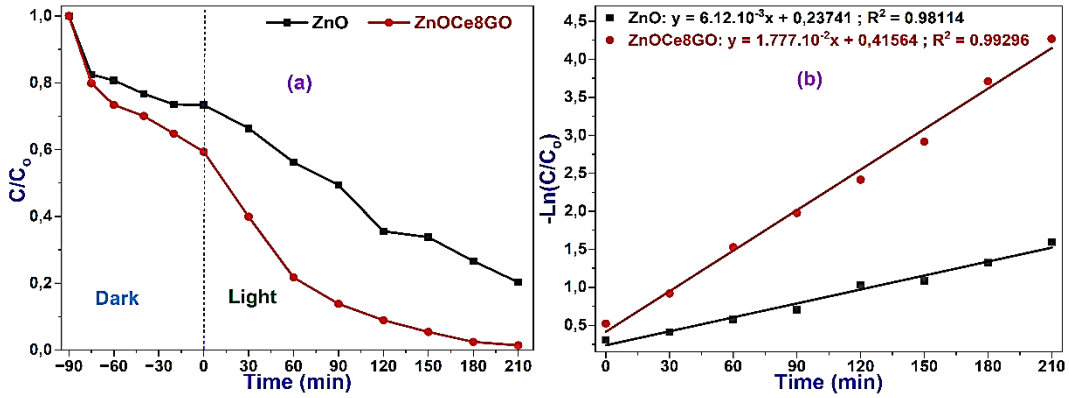

Figure 6. *Photocatalytic degradation of DR152: (a) C/C₀ variation and (b) kinetic plots.*

According to XRD analysis (Section 3.1), although the crystal size increased from 28.24 nm to 38.46 nm, which is usually accompanied by a decrease in specific surface area, the photocatalytic activity of the nanocomposites was still significantly improved. This is not at all contradictory, because: (i) Photocatalytic performance is primarily determined by the charge separation efficiency and not solely by the surface area; (ii) PL results confirm strong inhibition of electron–hole recombination; (iii) The narrowing of the band gap (3.15 → 2.78 eV) increases the absorption of visible light and (iv) GO acts as an electron conduction pathway.

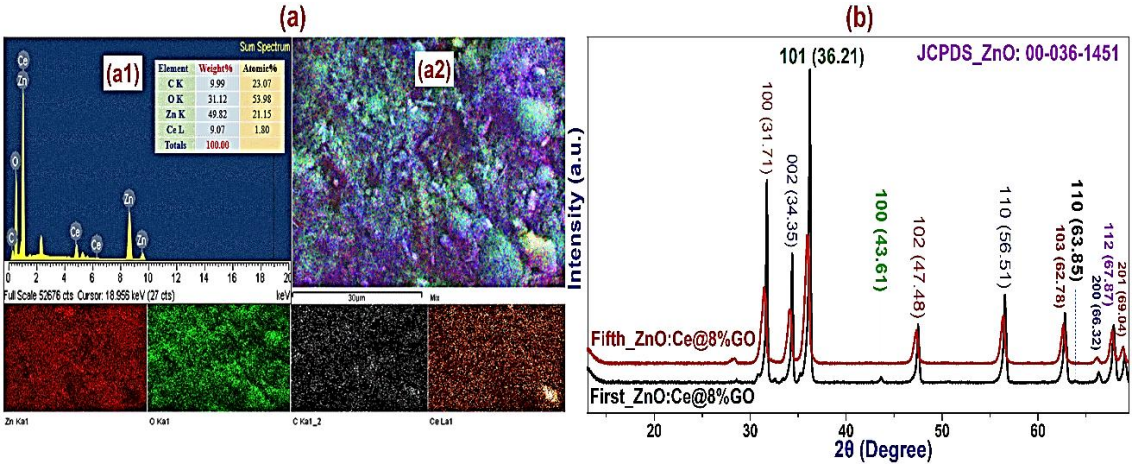

Figure 7. *(a) EDS spectra and (b) XRD pattern of ZnO:Ce@8%GO after five cycles.*

The EDS spectrum (Figure 7 a1) confirms that the original ZnO:Ce@8%GO sample contains only four main elements: Zn, O, C, and Ce, with a total mass of 100%. The element distribution image (Figure 7 a2) further demonstrates the uniform spatial distribution of Zn, O, C, and Ce. These results confirm the composition and uniform distribution in the structure of the ZnO:Ce@GO photocatalyst.

After 5 cycles of use, the ZnO:Ce@8%GO nanocomposite maintained a photocatalytic degradation efficiency of 83.71% for DR152 dye. The XRD patterns of ZnO:Ce@8%GO initial and after five cycles (Figure 7b) exhibits diffraction peaks consistent with the hexagonal wurtzite ZnO structure (JCPDS No. 00-036-1451). No new crystalline phases or impurity peaks are observed, indicating structural stability during photocatalytic reactions. The peak positions remain nearly unchanged, suggesting that the lattice structure is preserved after repeated use. Slight variations in peak intensity may be attributed to minor surface adsorption effects. Overall, the material maintains its crystallinity and phase integrity after cycling.

Table 2. *Comparison of the efficiency and dye treatment conditions of ZnO:Ce@8%GO nanocomposites with some related materials.*

Material	Organic colorants	Efficiency	Lighting conditions	Ref.
Ce-ZnO/rGO	Bromothymol blue	92.00%	Visible	[5]
GO-ZnO/Mn_2O_3	Malachite green	98.75%	Sunlight	[9]
Pr-ZnO	Organic pollutants	95.00%	Visible	[13]
ZnO:Ce@GO	Disperse red 152	98.60%	Visible	This work

4. CONCLUSIONS

ZnO and ZnO:Ce@(0–8)%GO nanocomposites were synthesized hydrothermally with crystallite sizes of 28–38 nm. Structural analyses confirmed the wurtzite ZnO phase and successful incorporation of Ce and GO. The absorption edge red-shifted from 394 to 446 nm, accompanied by band-gap narrowing from 3.15 to 2.78 eV. Significant PL quenching indicated enhanced charge

separation and reduced electron–hole recombination. Consequently, ZnO:Ce@8%GO achieved 98.60% degradation of Disperse Red 152 within 210 min, with a reaction rate 2.94 times higher than that of pristine ZnO and 83.71% efficiency after five cycles. These results demonstrate the synergistic effect of Ce and GO in improving visible-light photocatalytic performance.

Acknowledgments: *This work was conducted as part of a student research project for the 2025–2026 academic year at Thai Nguyen University of Education.*

REFERENCES

[1]. Z. Abdi, S. A. Zargar, O. Bagheri, R. A. Dolatsara, and A. M. Khachatourian, *"Preparation of rod-like Ni-doped ZnO anchored onto N-doped graphene nanosheets for pharmaceutical pollutant removal and evaluation of phytotoxicity"*, Materials Science in Semiconductor Processing, Vol. 188, pp. 1–16, (2025). doi: 10.1016/j.mssp.2024.109205.

[2]. N. F. Bappy and S. Subramani, *"A comprehensive review on Mg-doped ZnO thin film and nanostructure: Properties and applications"*, Materials Science and Engineering B, Vol. 318, pp. 1–39, (2025). doi: 10.1016/j.mseb.2025.118251.

[3]. S. Utara, N. Salidkul, A. Karaphun, S. Sonsupap, N. Chanlek, S. Hunpratub, and S. Phokha, *"Structural, morphological, optical, and electrochemical properties of Zn-doped CeO2/rGO nanocomposites"*, Materials Science in Semiconductor Processing, Vol. 189, pp. 1–16, (2025). doi: 10.1016/j.mssp.2025.109288.

[4]. K. Choudhary, R. Saini, and L. P. Purohit, *"Controllable synthesis of Ce-doped ZnO:TiO2 nanospheres for photocatalytic degradation of MB dye and levofloxacin under sunlight irradiation"*, Optical Materials, Vol. 143, pp. 1–9, (2023). doi: 10.1016/j.optmat.2023.114167.

[5]. M. Haruna, F. Eshun, C. K. Bandoh, E. S. Agorku, F. Opoku, N. K. Asare-Donkor, and A. A. Adimado, *"Binary Ce-doped-ZnO/rGO composite as excellent photocatalyst for bromothymol blue dye degradation"*, Sustainable Chemistry for the Environment, Vol. 5, pp. 1–8, (2024). doi: 10.1016/j.scenv.2024.100069.

[6]. Y. N. Patil and S. T. Nandibewoor, *"Development of novel Ce doped ZnO/graphene based sensor for electrochemical investigation of potassium-competitive acid blocker: Vonoprazan"*, Materials Science in Semiconductor Processing, Vol. 171, pp. 1–13, (2024). doi: 10.1016/j.mssp.2023.108039.

[7]. S. Choudhary, K. P. Sooraj, M. Ranjan, and S. Mohapatra, *"Facile fabrication of Au nanoparticles loaded Ce doped ZnO nanorods for efficient catalytic and photocatalytic decomposition of toxic pollutants in water"*, Inorganic Chemistry Communications, Vol. 165, pp. 1–17, (2024). doi: 10.1016/j.inoche.2024.112482.

[8]. M. Elahian, N. Ahmadi, A. A. Heidari, N. Mengelizadeh, and D. Balarak, *"Preparation of a polyaniline-supported Ce-Ag-doped ZnO nanocomposite for efficient photocatalytic degradation of acid blue 113 dye"*, Results in Engineering, Vol. 25, pp. 1–12, (2025). doi: 10.1016/j.rineng.2024.103824.

[9]. D. R. Rout, S. Chaurasia, and H. M. Jena, *"Enhanced photocatalytic degradation of malachite green using manganese oxide doped graphene oxide/zinc oxide (GO-ZnO/Mn2O3) ternary composite under sunlight irradiation"*, Journal of Environmental Management, Vol. 318, pp. 1–14, (2022). doi: 10.1016/j.jenvman.2022.115449.

[10]. A. Mahesha, M. Nagaraja, A. Madhu, N. Suriyamurthy, S. S. Reddy, M. Al-Dossari, N. S. Abd EL-Gawaad, S. O. Manjunatha, K. Gurushantha, and N. Srinatha, *"Chromium-doped ZnO nanoparticles synthesized via auto-combustion: Evaluation of concentration-dependent structural, band gap-narrowing effect, luminescence properties and photocatalytic activity"*, Ceramics International, Vol. 49, pp. 22890–22901, (2023). doi: 10.1016/j.ceramint.2023.04.113.

[11]. A. Kamaraj, C. Ragavendran, S. Naveenkumar, K. A. Al-Ghanim, A. Priyadharsan, and C. Vetrivel, *"Green synthesized yttrium-doped ZnO nanoparticles: A multifaceted approach to mosquito control, antibacterial activity, cytotoxic properties of liver cancer cells, and photocatalytic properties"*, Inorganic Chemistry Communications, Vol. 176, pp. 1–19, (2025). doi: 10.1016/j.inoche.2025.114225.

[12]. M. Haruna, C. K. Bandoh, E. S. Agorku, F. Opoku, N. K. Asare-Donkor, and A. A. Adimado, *"Experimental and ab initio studies of enhance photocatalytic efficiency of La-doped ZnO/g-C3N4 nanocomposites for bromothymol blue dye degradation"*, Next Materials, Vol. 4, pp. 1–11, (2024). doi: 10.1016/j.nxmate.2024.100212.

[13]. C. Cojocaru, P. Pascariu, C. Romanitan, M. Silion, P. Samoila, and A. B. Serban, *"Intensification of organic pollutant degradation under visible light irradiation using ZnO nanostructured photocatalysts doped with praseodymium"*, Applied Surface Science, Vol. 661, pp. 1–16, (2024). doi: 10.1016/j.apsusc.2024.160042.

[14]. D. Parashar, G. Achari, and M. Kumar, *"Facile synthesis of silver doped ZnO nanoparticles by thermal decomposition method for photocatalytic degradation of metronidazole under visible light"*, Journal of Environmental Chemical Engineering, Vol. 12, pp. 1–15, (2024). doi: 10.1016/j.jece.2024.113205.

[15]. X. Dong, X. Yu, X. Zhang, Z. Zhang, X. He, R. Wei, Y. Bai, and J. Fan, *"Synthesis of Tb-doped ZnO/RGO nanocomposites and its enhanced photocatalytic activity under visible light irradiation"*, Diamond & Related Materials, Vol. 133, pp. 1–13, (2023). doi: 10.1016/j.diamond.2023.109765.

TÓM TẮT

Vật liệu nanocomposite ZnO:Ce@GO tiên tiến nhằm tăng cường hoạt tính quang xúc tác phân hủy thuốc nhuộm Disperse Red 152 dưới ánh sáng khả kiến

Các vật liệu nano tổng hợp ZnO và ZnO:Ce@(0–8)%GO được tổng hợp bằng phương pháp thủy nhiệt và được đặc trưng bằng XRD, FT–IR, PL, EDS và UV–Vis–DRS. Các vật liệu này vẫn giữ cấu trúc wurtzite của ZnO với kích thước tinh thể từ 28–38 nm. Việc pha tạp Ce và kết hợp GO đã làm giảm khoảng cách vùng cấm từ 3,15 xuống 2,78 eV và ức chế đáng kể sự tái kết hợp electron-lỗ trống, được chứng minh bằng sự dập tắt PL. Dưới bức xạ ánh sáng nhìn thấy, ZnO:Ce@8%GO đạt được hiệu quả phân hủy DR152 là 98,60% sau 210 phút, so với 79,69% đối với ZnO nguyên chất, với tốc độ phản ứng cao hơn 2,94 lần. Vật liệu tổng hợp này cũng giữ được 83,71% hoạt tính sau năm chu kỳ, chứng tỏ độ ổn định tốt và sự tăng cường hiệp đồng hiệu suất quang xúc tác bởi Ce và GO.

Từ khóa: ZnO:Ce@GO; Nanocomposite; Hiệu ứng hiệp đồng; Quang xúc tác; Disperse Red 152.